Polymer Journal (2019) 51:579–590
https://doi.org/10.1038/s41428-018-0167-y

ORIGINAL ARTICLE

Shape memory conductive electrospun PVA/MWCNT nanocomposite aerogels

Maryam Heidarshenas[1] · Mehrdad Kokabi[1] · Hadi Hosseini[1]

Received: 24 October 2018 / Revised: 10 December 2018 / Accepted: 10 December 2018 / Published online: 17 January 2019

Abstract

Shape memory polymers have promising applications in different fields. In this work, polyvinyl alcohol/multiwall carbon nanotube nanocomposite aerogels were fabricated through supercritical CO_2 drying of electrospun hydrogel counterparts. Mercury porosimetry measurements and scanning electron microscopy results indicated that the nanofibrous aerogel had a high porosity (more than 80%), low density (0.025–0.036 g cm^{-3}), high surface area (more than 1700 m^2 g^{-1}) and a pore size less than 100 nm. By incorporating multiwall carbon nanotubes, the density and Young's modulus of the polyvinyl alcohol/multiwall carbon nanotube nanocomposite aerogel were increased up to 0.03 g cm^{-3} and 38 MPa, respectively. A percolation threshold of 1.5 wt% of the multiwall carbon nanotube was achieved for the conductive polyvinyl alcohol/multiwall carbon nanotube nanocomposite aerogel. The nanofibrous aerogel showed a perfect shape memory effect under thermal stimulus, and the corresponding results revealed that the shape recovery ratio and recovery speed of the nanocomposite aerogel were significantly higher than pure polyvinyl alcohol aerogel owing to the stabilizing of the crystalline domains and improvements in mechanical properties due to the presence of the multiwall carbon nanotubes.

Introduction

Shape memory polymer (SMP) is a new kind of smart material that can switch from its permanent shape to a temporary shape upon the application of an external force and while heating above its transition temperature [1]. SMP has promising applications in a variety of fields that include aerospace [2], smart textiles [3], medicine [4], electronics, sensors, and actuators [5]. The typical SMP is inexpensive and lightweight and can remember very high strain values, making it an alternative to shape memory alloys and shape memory ceramics [6]. However, the strength and stiffness of SMP are low, and its shape recovery stress is not noteworthy. To improve the mechanical properties of SMPs and to develop new functionality in this system, SMP-based nanocomposites were developed [7].

Polyvinyl alcohol (PVA) exhibits efficient shape memory behavior in addition to biocompatibility, high hydrophilicity and nontoxicity [8]. PVA, similar to other SMPs, has two parts: switching segments (soft segments) and net points (hard segments). Crystal domains and crosslinked networks constitute net points, whereas amorphous domains form switching segments. The shape memory effect of PVA can change based on the degree of crosslinking [9].

Du et al. [9] fabricated PVA/acidic multiwall carbon nanotube films through traditional solution casting, yielding films that exhibited good shape memory behavior in the dry state. The incorporation of multiwall carbon nanotubes (MWCNTs) had a significant effect on the shape recovery behavior of the system due to the strong interactions between the MWCNTs and both the hard and soft segments of PVA; similarly, the nanotubes were able to enhance the strength and stiffness of neat shape memory polymer. To extend the application range of PVA, Du et al. [10] prepared chemically cross-linked PVA films using glutaraldehyde. The prepared PVA film contained a small amount of water molecules, which enhanced the shape memory behavior of the PVA. In fact, additional water molecules acted as plasticizers, thereby increasing the mobility of the soft segments. As a result, the T_g of the film sharply decreased to

✉ Mehrdad Kokabi
mehrir@modares.ac.ir

[1] Department of Polymer Engineering, Faculty of Chemical Engineering, Tarbiat Modares University, P.O. Box 14115-114 Tehran, Islamic Republic of Iran

room temperature. Shape memory PVA-matrix nanocomposites exhibited better performance compared to their neat polymer counterpart. Miaudet et al. [11] focused on PVA/single wall carbon nanotube (SWCNT) fibers prepared by a particular coagulation spinning process. Their system showed a strong shape memory effect due to the effective presence of the SWCNTs and developed a shape recovery stress that was up to two orders of magnitude greater in comparison with the neat polymer counterpart. Zhong et al. [12] manufactured carbon nanotube-reinforced PVA fibers using the wet-spinning method. The produced shape memory fibers were used as a smart substrate for highly flexible fibrous supercapacitors and were found to exhibit shape memory behavior and excellent energy storage efficiency. Basfar et al. [13] investigated the shape memory behavior of PVA/MWCNT films in hot water. The films were crosslinked by glutaraldehyde in the presence of 2-carboxyethyl acrylate oligomers (CEA), then exposed to ionizing radiation for more crosslinking. Due to the strong interaction between the crosslinked PVA/MWCNT nanocomposite and water, this material showed shape recovery at a shorter time than crosslinked neat PVA. Du et al. [14] conducted another survey of PVA/MWCNT nanocomposite films under electrical stimulation. By applying a constant voltage of 60 V, the optimized sample was able to recover its permanent shape within 35 s. Wang et al. [15] prepared a multistimuli (water-responsive and thermoresponsive) shape memory PVA-graft-polyurethane (PU) film. The presence of the PU segment provided a physical crosslinking around the PVA segment and exhibited a thermoresponsive shape memory effect. The PVA segments developed a wide transition temperature range and indicated a water-induced shape memory effect. Chen et al. [16] synthesized PVA/tannic acid (TA) hydrogels that showed an outstanding shape memory effect in hot water. TA, as a plant-derived polyphenol with many functional groups, can create strong H-bonds with PVA. The stronger H-bonds between PVA and TA act as permanent crosslinks, and the weaker H-bonds, as temporary crosslinks, allowing the system to exhibit shape memory behavior. All of the mentioned systems are hydrogels, fibers or films, and based on our knowledge, a shape memory nanocomposite aerogel based on PVA has not yet been studied. An aerogel is a highly porous solid [17] with distinct properties such as a low density (0.01–0.3 $g\,cm^{-3}$), high porosity (>80%) [18], and high specific surface area (400–1100 $m^2\,g^{-1}$) [19], but poor mechanical properties [20]. Some researchers have focused on polymeric [21] and nanofibrous flexible [22, 23] aerogels to overcome the fragility typically found in these materials. These lightweight shape memory materials can display unique applications in many fields such as aerospace or biomedical [2]. In this work, shape memory polymeric nanocomposite aerogels based on electrospun PVA/MWCNT were developed to achieve flexibility, electrical conductivity, and the desired shape memory performance. PVA/MWCNT nanofibrous hydrogels were prepared and subsequently dried using the supercritical CO_2 ($ScCO_2$) drying method to obtain nanocomposite aerogels. The fabricated PVA/MWCNT nanofibrous nanocomposite aerogels were characterized via scanning electron microscopy (SEM), mercury porosimetry, and dynamic mechanical thermal analysis. Moreover, the electrical conductivity and shape memory effect of the harvested aerogels were examined.

Materials and methods

PVA (polymerization degree = 1700 and saponification value ≥ 98%) was purchased from the Nippon Synthetic Chemical Industry Co., Ltd., Japan. Acid-treated MWCNTs were supplied by the Research Institute of the Petroleum Industry of Iran and had characteristic diameter and length values of 10–20 nm and 5–15 μm, respectively. All of the materials were used without further purification.

Electrospinning of the PVA and PVA/MWCNT solutions

PVA solution (5.5 wt%) was prepared by dissolving PVA powder in distilled water at 80–90 °C for 1 h. The homogenous solution was then transferred to a 20 mL plastic syringe with a diameter of 19 mm attached to a 22-gauge needle, which was then inserted into the electrospinning apparatus (A Harvard syringe pump, PHD 2000, USA). Then, the PVA solution was electrospun onto a steady metallic collector at room temperature. To prepare the PVA/MWCNT solution, 1 wt% of sodium dodecyl sulfate (SDS) was dissolved in distilled water using a magnetic stirrer for 1 h at room temperature. Then, different fractions of MWCNTs were sonicated into this solution for 0.5 h. Finally, PVA powder was added and dissolved for approximately 2 h at 80 °C until a homogenous solution was reached. All electrospinning procedures were carried out in a clean room.

Preparation of the aerogels

The freeze-thawed electrospun PVA and PVA/MWCNT fibrous hydrogels were dried in a homemade high-pressure $ScCO_2$ drying unit after thrice exchanging the ethanol solvent. To promote physical crosslinking and strengthen the samples against water, all of the samples were then placed in an oven at 110 °C for 16 h.

Characterization of the aerogels

The morphological appearance of the electrospun PVA nanofiber aerogels was investigated by SEM (AIS2100, Seron Technology). The average nanofiber diameter was calculated from SEM micrograph measurements of 30 fibers using Axio Vision software.

The bulk densities of the aerogels were determined by weighing the samples and measuring their volumes. The measurement was repeated thrice for each of five sample types.

The porosity of the aerogel was calculated by gravimetric measurement, as shown by Eq. (1):

$$\text{Porosity}\,(\%) = \left(1 - \frac{\rho}{\omega_{\text{PVA}}\rho_{s,\text{PVA}} + \omega_{\text{MWCNT}}\rho_{s,\text{MWCNT}}}\right) \times 100, \tag{1}$$

where ρ, $\rho_{s,\text{PVA}}$ and $\rho_{s,\text{MWCNT}}$ are the densities of the nanocomposite aerogel, the skeletal density of the pure PVA, and the skeletal density of the MWCNT, respectively. The parameters ω_{PVA} and ω_{MWCNT} are the mass fractions of PVA and MWCNT in the nanocomposite aerogels, respectively. Herein, based on the literature data, $\rho_{s,\text{PVA}}$ and $\rho_{s,\text{MWCNT}}$ were fixed to 1.31 g cm^{-3} and 2.1 g cm^{-3}, respectively. Five measurements were collected for each formulation, and the average values and the standard deviations were reported.

In addition, mercury porosimetry (PASCAL 440 Thermo Finnigan, Italy) was applied to analyze the porous structure of all aerogel specimens. The pore size of an aerogel beyond its critical pressure (P_c) can be obtained according to the Washburn equation, Eq. (2):

$$r = \frac{-2\gamma\cos\theta}{P} \tag{2}$$

For pressures below the P_c, the aerogel samples collapse, and thus, the Pirard's theory could be considered, as shown by Eq. (3):

$$2r = \frac{k_f}{P^{0.25}}, \tag{3}$$

where k_f is the buckling constant defined by Eq. (4):

$$k_f = \frac{4\gamma\cos\theta}{P_c^{0.75}} \tag{4}$$

Moreover, it has been reported that the Young's moduli of aerogel specimens can be determined using mercury porosimetry results via the equation immediately below [24]. Accordingly, the bulk moduli of the specimens were calculated using the early stage of mercury pressure, as shown by Eq. (5):

$$K = \frac{1}{\rho_b}\beta \tag{5}$$

In the above formula, ρ_b (g cm^{-3}) and β (MPa g cm^{-3}) denote the bulk density and the average slope of the pressure P against the volume variation ΔV curve (for P less than P_c), respectively. Then, Young's modulus can be determined by Eq. (6):

$$E = 3(1 - 2\upsilon)K \tag{6}$$

The Poisson's ratios of PVA and carbon nanotube are generally considered to be 0.44 and 0.2, respectively [25].

To determine the gel content, each type of sample was completely dried after reaching a stable weight of m_i. Then, each dried sample was floated on distilled water to dissolve the uncrosslinked portions. Afterward, each sample was once more dried until the stable weight of m_f was obtained. Finally, the gel content was calculated by Eq. (7):

$$\text{Gel content}\,(\%) = \frac{m_f}{m_i} \times 100 \tag{7}$$

The electrical conductivity of PVA aerogels with different loading levels of MWCNTs was measured using a broadband dielectric spectrometer, GW Instek (LCR-8101G LCR meter-Taiwan) under both DC and AC modes at room temperature. To determine the percolation threshold, aerogels containing 1–3 wt% of MWCNT were prepared. To remove the influence of the contact resistance between the sample and the probe, copper tape was applied at both ends of the sample. Electrical conductivity can be calculated in DC mode according to Eq. (8):

$$\sigma = \frac{d}{RA}, \tag{8}$$

where σ is the electrical conductivity, R is the resistivity, d is the thickness, and A is the surface area of the sample. Furthermore, AC electrical conductivity investigations were carried out at frequencies of 20 Hz to 10^6 MHz.

Dynamic mechanical thermal analysis (DMTA) was employed to investigate pure PVA aerogel and PVA containing 1.5 wt% MWCNT nanocomposite aerogel in the tension mode (NETZCH-242C). The samples were cut into rectangular strips with dimensions of approximately 20 × 5 × 0.2 mm^3, and then, DMTA was performed at 25–150 °C with a heating rate of 5 °C min^{-1} at a frequency of 1 Hz.

The shape memory behavior of the aerogels was examined using a bending test under the thermally activated condition for 3 cycles. The strip-like samples had a maximum length of 40 mm, a maximum width of 5 mm and a thickness of 0.2 mm. The samples were first heated to a temperature greater than the material's transition temperature (98 °C) and, then, were deformed by bending and quickly cooled to room temperature to set the deformed shape. Afterward, the deformed samples were heated up to the recovery temperature (90 and 95 °C), allowing the shape of each sample to gradually return to the primary shape. The

shape recovery ratio R_r and shape recovery speed R_s can be calculated by Eqs. (9) and (10):

$$R_r = \frac{\theta_t - \theta_0}{180 - \theta_0} \times 100\%, \quad (9)$$

$$R_s = \frac{\theta_t - \theta_0}{t}, \quad (10)$$

where Θ_0 and Θ_t represent the primary bending angle of the deformed sample and recovery angle of the sample at recovery time t during the recovery process, respectively [26].

Results and discussion

Morphology and microstructure

The nanofiber morphology was influenced by different variables, such as the solution concentration and surface tension, flow rate, applied voltage and tip-to-target distance during electrospinning. Prior to electrospinning the PVA/MWCNT solutions, the spinning system was tuned to accommodate the pure PVA solution to produce PVA nanofibers. The conditions obtained were as follows: PVA concentration = 5.5 wt%, flow rate = 0.2 mL/h, applied voltage = 19 kV, and tip-to-target distance = 16 cm. These desirable conditions yielded smooth and uniform bead-free PVA nanofibers with an average diameter of 85 ± 5 nm, as shown in Fig. 1a. According to SEM micrographs (Fig. 1a–d); all aerogel specimens revealed 3D nanofibrous networks associated with an interconnected highly porous framework. This structure was preserved despite loading with MWCNT fractions. The PVA/MWCNT solutions were electrospun under identical conditions, except for the voltage. Due to the presence of MWCNTs, the solution was conductive, thus the voltage was reduced to 15 kV. According to SEM micrographs, the average nanofiber diameters decreased to the 60–75 nm upon the incorporation of MWCNTs. The PVA/MWCNT (1.0 wt%) nanofibers were observed to have the smallest diameters due to the enhanced electrical conductivity of the solution (Fig. 1b). The conductive nature of the PVA/MWCNT solution reduced the electrostatic potential, giving thinner or smaller diameter filaments during the electrospinning process [27]. Nevertheless, as the nanotube content was increased to 2.0 wt% and then 3.0 wt%, the average diameter of the resulting nanofibers increased slightly. This observation was attributed to the agglomeration of the MWCNTs, which were not wrapped by the PVA matrix; this fact led to the distortion of the nanofibers (Fig. 1c, d). This observation has been previously reported by other researchers studying electrospun nanofibers containing MWCNTs [27, 28]. The average diameter of the nanofibers in all of the samples was less than 100 nm.

The variation of the bulk density and shrinkage relative to MWCNT content is shown in Fig. 2a. The apparent densities of the PVA aerogel and its nanocomposite aerogel counterparts were in the range of 0.0254–0.0364 g cm^{-3}. In addition, the porosity of the fabricated neat PVA aerogel, as well as that of the PVA/MWCNT nanocomposite aerogels, was higher than 80%, as listed in Table 1. This implied that lightweight aerogels with high porosities had been successfully prepared. Nevertheless, by incorporating MWCNTs into the PVA matrix, the density of the resulting material was slightly increased. This fact was attributed to the increased amount of solid content in the aerogel specimens due to loading with the MWCNTs and the comparatively higher density of carbon nanotubes (2.1 g cm^{-3}) compared to that of PVA (1.3 g cm^{-3}). Furthermore, as observed in Table 1, increasing the MWCNT concentration led to the formation of a denser aerogel with reduced porosity. Moreover, all aerogel specimens revealed a small amount of shrinkage due to the use of $ScCO_2$, which is an efficient drying method. When using this drying method, the effect of capillary forces can be eliminated. Upon increasing the MWCNT content, the shrinkage of the nanocomposite aerogels upon drying gradually decreases. This observation suggested that the presence of MWCNTs in the PVA framework endowed the nanocomposite material with a more robust structure that was thereby able to overcome capillary forces. Dourani et al. [29] also observed reduced nanocomposite aerogel shrinkage upon loading with nanotubes. According to these findings, the density and pore structure of PVA and its nanocomposite aerogel specimens can be controlled by the MWCNT concentration of the initial PVA solution.

To further clarify the porous microstructure of the harvested aerogels, mercury porosimetry was employed. Figure 2b depicts the porosimetry curves obtained for PVA and the PVA/MWCNT nanocomposite aerogels. All samples exhibited a nonclassical behavior under exposure to mercury porosimetry pressure. According to the pressurization curve, two successive behaviors can be observed. At a low pressure, the sample collapsed under the pressure of the mercury, and then, beyond the transition pressure value (P_c), mercury began to penetrate the small pores of the network instead of crushing the network structure. The P_c value can easily be recognized as a steep increase in the volume versus pressure curve. This critical pressure value divides the curve into two separate parts, which are distinguished by this sudden change. The P_c values were calculated as 35, 80, 50, and 40 MPa for PVA aerogel, PVA/MWCNT (1 wt%), PVA/MWCNT (2 wt%) and PVA/MWCNT (3 wt%) nanocomposite aerogels, respectively. According to the estimated P_c, the buckling constant k_f was

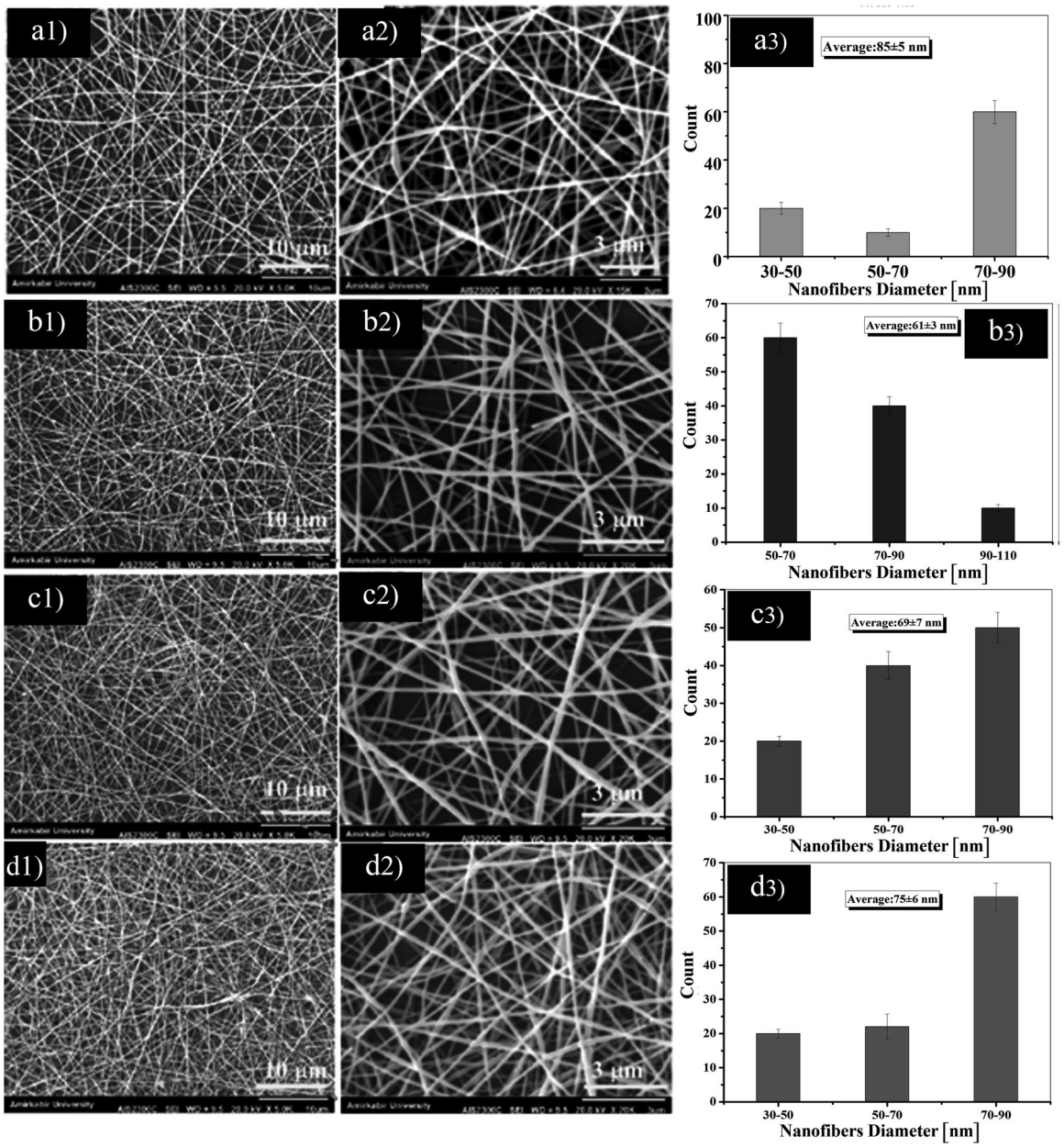

Fig. 1 SEM micrographs and distribution of the nanofiber diameters for **a** PVA aerogel and **b** the PVA-MWCNT (1 wt%), **c** PVA-MWCNT (2 wt %), and **d** PVA-MWCNT (3 wt%) nanocomposite aerogels

computed for all of the samples. The determined results are listed in Table 2. At transient pressure, P_c, both the Washburn intrusion and Pirard collapse theories were simultaneously reliable. The pore size distribution results indicated the accumulation of mesopores in the harvested aerogels (Fig. 2c).

The specific surface area findings of the aerogels are summarized in Table 2. Accordingly, the surface area of the aerogels prepared using the $ScCO_2$ drying method was higher than those of previously reported aerogels prepared by the freeze-drying process due to the enhanced preservation of the initial hydrogel network structure during the supercritical drying process [30]. In this regard, a specific surface area value of 157 m^2/g was reported for freeze-dried PVA-MWCNT [31], a value that is significantly lower than that of the PVA/MWCNT nanofibrous aerogels fabricated in the present work. As shown in Table 2, by increasing the MWCNT content, the specific surface area (obtained by mercury porosimetry) of the aerogel decreased. This phenomenon was related to the presence of a large amount of MWCNTs in the PVA nanofiber mat; the MWCNTs compressed the nanofiber skeleton and reduced its porosity. This observation was in agreement with the findings of Worsley et al. [32] and Kohlmeyer et al. [33]. As these authors

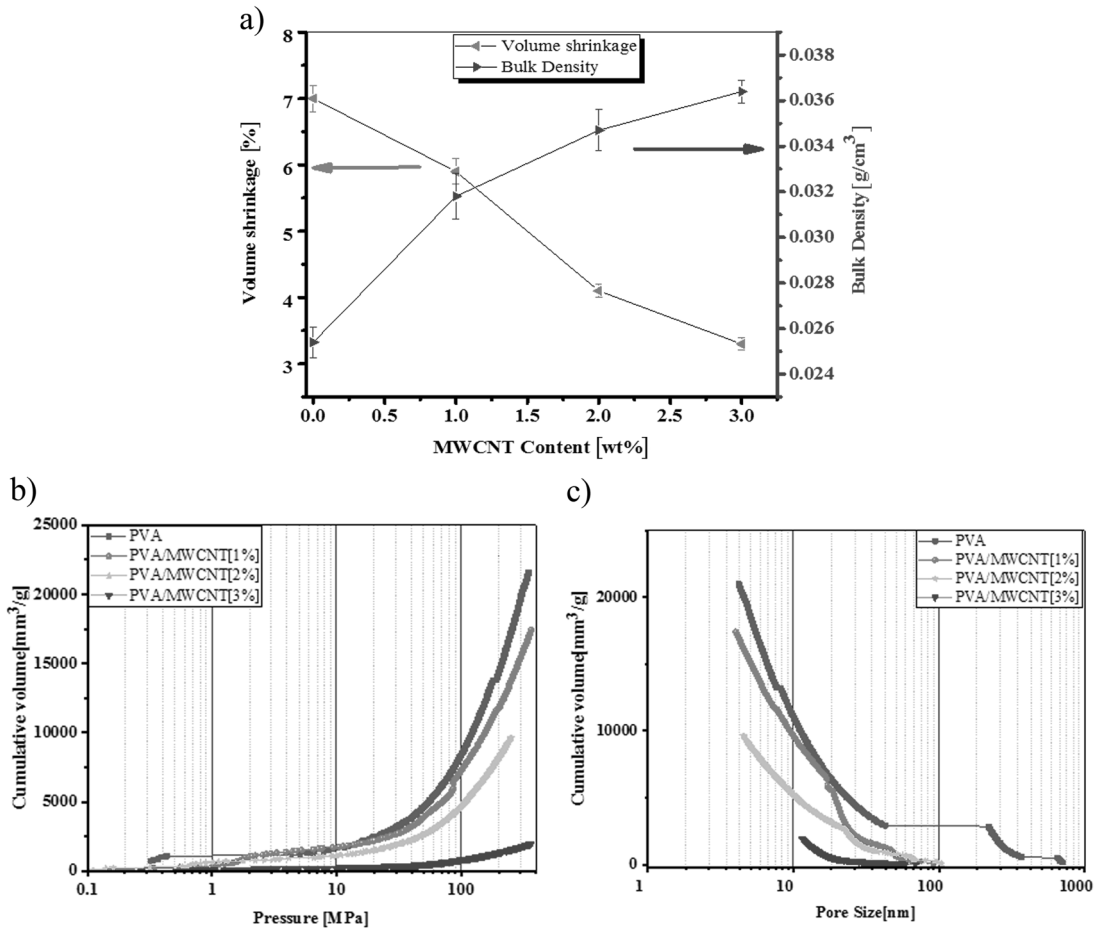

Fig. 2 **a** The variation of density and shrinkage with the MWCNT content, **b** cumulative volume versus pressure, **c** cumulative pore volume versus pore size

Table 1 Physical and porous texture properties of the fabricated aerogel specimens

Sample	P (g cm^{-3})	P (%)	da (nm)
PVA	0.0254 ± 0.050	90.88 ± 4.024	85 ± 5
PVA-MWCNT (1 wt%)	0.0318 ± 0.042	84.94 ± 3.35	61 ± 3
PVA-MWCNT (2 wt%)	0.0347 ± 0.034	83.19 ± 3.49	69 ± 7
PVA-MWCNT (3 wt%)	0.0364 ± 0.046	83.10 ± 2.76	75 ± 6

da is the average nanofiber diameter

expressed with regard to loading aerogels with MWCNTs, both micropores and mesopores become blocked, thereby considerably reducing the surface area of the harvested nanocomposite aerogels.

The compressive behavior of the harvested aerogels was obtained via mercury porosimetry, according to the previously procedure. The results are summarized in Table 2. As observed, by incorporating the carbon nanotubes into the PVA framework, Young's modulus was increased from 3.6 MPa for the neat PVA aerogel up to 38 MPa for the nanocomposite aerogel containing 3 wt% MWCNT. This trend was attributed to the reinforcing effect of carbon nanotubes, which is associated with the good interaction between the PVA functional groups and those of the carbon nanotubes.

Electrical conductivity of aerogels

The broad-band electrical conductivity is recognized as $\sigma = \sigma_{DC} + \sigma_{AC}$, where σ_{DC} and σ_{AC} are the electrical conductivity in direct current and alternating current conditions, respectively. Generally, σ_{DC} is independent of frequency and instead originates from the motion of electrons under the application of an electric field. In contrast, σ_{AC} is generated by dipole rotation and reorientation in alternating fields that are ascribed to the effect of polarization. In this regard, AC conductivity is a powerful tool for studying the relaxation behaviors of conductive, semiconductive and insulating materials [34]. In addition, this method can be employed to further evaluate the constituted conductive networks and related fractal dimensions.

The DC electrical conductivity of the aerogels with respect to the MWCNT loading level is represented in Fig. 3a. The

Table 2 Porous structural properties of PVA aerogel and PVA/MWCNT nanocomposite aerogels

Sample	Specific surface area (m^2/g)	Average pore size (nm)	k_f (nm MPa $^{0.25}$)	Pc (MPa)	Young's modulus (MPa)
PVA	17351	5	530	35	3.6 ± 0.5
PVA-MWCNT (1 wt.%)	6987	4	56	80	14.2 ± 1.1
PVA-MWCNT (2 wt.%)	4289	7	80	50	29.7 ± 2.3
PVA-MWCNT (3 wt.%)	1792	5	93	40	38.5 ± 1.7

electrical conductivity of pure PVA was 1.25×10^{-13} S cm^{-1}. The electrical conductivity increased by approximately two orders of magnitude (2.85×10^{-11} S cm^{-1}) upon loading the PVA matrix with 1 wt% of MWCNT. This finding indicated that the PVA/MWCNT aerogel was still in the insulating state. When the MWCNT content was increased to 1.5 wt%, the electrical conductivity soared abruptly by four orders of magnitude, i.e., 3.62×10^{-7} S cm^{-1}. This result implied that the conductive carbon nanotubes had created a continuous pathway, as well as a percolation network, which resulted in the movement of electrons throughout the conductive network, following a metal-like behavioral transition in the continuous pathway [35]. By further increasing the MWCNT content, the electrical conductivity remained almost steady and constant, confirming the formation of a stable and conductive network of carbon nanotubes. These findings indicated that the fabricated nanocomposite aerogels exhibited a percolated behavior. The conductivity of a nanocomposite based on conductor-insulator components obeys a power law behavior in the form of $\sigma \propto (\phi\text{-}\phi_c)^t$, where σ is the nanocomposite aerogel conductivity, ϕ and ϕ_c are the MWCNT content and percolation threshold, respectively, and t is the critical exponent. A log–log plot of σ against $(\phi\text{-}\phi_c)/\phi_c$ is depicted in the inset of Fig. 3a; taking $\phi_c \sim 1.6$ wt% and $t = 1.02$ gives a relatively good fit to the data. It has previously been reported that t, the universal critical exponent, depends on the dimensions of the conductive network. Therefore, a value of 1 for t indicates the formation of two-dimensional carbon nanotube conductive networks [36].

The AC conductivity as a function of the frequency for aerogels containing different MWCNT loading levels is displayed in Fig. 3b. For the neat PVA and PVA/MWCNT nanocomposite aerogels with low MWCNT contents, beneath the percolation threshold, the conductivity curves indicated a strong dependence on frequency due to their insulating nature. Therefore, the plot of AC conductivity against frequency increased almost linearly with a slope in the range of 0.95–1. This behavior originated from the normal diffusion of charge carriers. As the MWCNT content exceeded 1.5 wt%, a plateau develops in the low-frequency range, following the linear increase of conductivity that was previously observed, revealing a transition from insulating to semiconducting behavior, due to the development of the first continuous conductive paths of

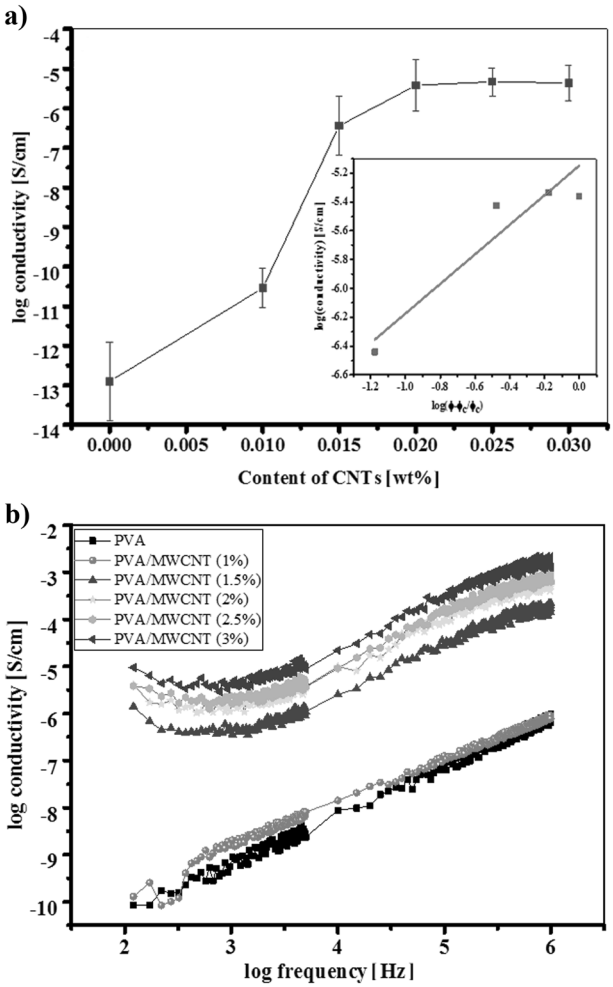

Fig. 3 Variation of **a** DC conductivity [inset shows log-log plot of conductivity vs. $(\phi\text{-}\phi_c/\phi_c)$] and **b** AC conductivity with MWCNT loading

carbon nanotubes. This behavior can be attributed to the anomalous diffusion of charge carriers. The slope of the conductivity curve in the high-frequency range was 0.79. Moreover, the frequency of ω_c is defined as the crossover frequency at which the AC conductivity ($\sigma_{ac}(\omega)$) diverges from the conductivity of the plateau region. According to the anomalous diffusion conduction mechanism, $\sigma_{ac} \propto \omega^n$ (for $\omega > \omega_c$) at which n is equal to the slope; hence, the fractal dimension of the nanofiller network can be determined using the formula $n = (d_w - d_f + 1)/d_w \cong 0.79$,

where d_w and d_f correlate with the anomalous diffusion exponent and fractal dimension, respectively. At the percolation threshold, the value of d_w is known to be equal to 3.8 [37]. Based on these explanations, the fractal dimension obtained (1.8) provided useful information regarding the structure of the nanofiller network. This value was far away from the fractal dimension of the carbon black-based filler network, i.e., 2.5, reported by Fritzsche et al. [37]. This finding indicated the establishment of different types of conductive networks in the presence of nanofillers with variable geometry. Furthermore, an abrupt increase in conductivity by up to 4 orders of magnitude was observed for the electrical percolation threshold and MWCNT network formation. Beyond the percolation threshold, the conductivity was frequency-independent and initially constant in the low-frequency range, then increased at higher frequencies, attributed to the dispersion region. The plateau region of the frequency-independent conductivity was related to the aerogel's DC conductivity. These results suggested that there was good agreement between the DC and AC conductivity outcomes.

Dynamic mechanical behavior of the aerogels

The variation of the storage modulus (E') and *tan* δ as functions of temperature for neat PVA aerogel and the PVA/MWCNT (1.5 wt%) nanocomposite aerogel is displayed in Fig. 4.

According to this figure, the storage modulus declined drastically with increasing temperature. Furthermore, the relaxation time of the polymer chains gradually decreased with temperature, leading to an increase in chain mobility. This relaxation behavior was attributed to the T_g of the polymer. For PVA/MWCNT nanocomposite aerogels, a dramatic enhancement of E' was observed throughout the entire temperature range, suggesting that the integration of MWCNTs into the PVA framework had a significant impact on the elastic properties of the PVA matrix. This finding confirmed that the reinforcement effects of PVA/MWCNT nanocomposite aerogels were predominated by the existence of MWCNTs and the development of possible interaction zones between the carboxylated-MWCNTs and PVA nanofibers. This phenomenon induced an interphase region of immobilized polymer coated on the embedded MWCNTs. Similar results were reported by Wu et al. [38] and Park et al. [39]. The interaction occurred between the PVA functional groups (hydroxyl groups) and the carboxyl groups of the MWCNTs. Another reason for enhanced storage modulus was a uniform distribution of the nanotubes at the nanoscale level. When the MWCNTs were added to the pure PVA as reinforcement, the nanocomposite modulus increased (Fig. 4a). Moreover, it was expected that the shape recovery stress associated with the shape memory effect would be improved with increasing modulus in the system. The dramatic decrease in the storage modulus contributed significantly to the observation of a good shape memory effect. The degree to which the systems exhibited thermosensitivity gave rise to a significant decline in the storage modulus, altering the material from a glassy state to a rubbery state.

The loss factors (*tan* δ) as functions of temperature for the PVA aerogel and PVA/MWCNT nanocomposite aerogel are illustrated in Fig. 4b. The loss factor peaked in the glass transition region because it was very sensitive to molecular motion. During the glass transition state, the movement of small functional groups was initiated in the polymer molecular chain. These small groups were initially frozen in place. When nanotubes were added to the PVA, the value of *tan* δ decreased, and the peak value shifted to a higher temperature. The incorporation of MWCNTs reduced the free volume between the PVA molecular chains and impeded their mobility, thereby increasing their relaxation temperature. As observed, the amount of *tan* δ in the PVA/MWCNT nanocomposite aerogel decreased in comparison with that of the PVA aerogel counterpart due to the uniform dispersion of nanotubes in the PVA matrix and the good interaction between the PVA functional groups (hydroxyl groups) with those of the MWCNTs (carboxylic acids and esters groups). As indicated by the *tan* δ curves, the presence of the MWCNTs caused T_g to increase from 45 to 85 °C. To describe the hydrogen bond interactions between the PVA molecules and MWCNT functional groups, a schematic illustration is presented in Fig. 5.

Shape memory behavior

The most important parameter for observing shape memory behavior is the physical crosslinking network associated with the insolubility of an aerogel and is determined by calculating the gel content. A chemical or physical crosslinking network is one of the two basic requirements of a polymer to exhibit SME. The other requirement is the existence of a reversible thermal transition, which is essential to fix the temporary shape and recover the permanent shape. Most polymers have this requirement despite having a melting point or glass transition temperature. In turn, if the crosslinking network can be created, then the shape memory effect will be observed. In the absence of crosslinking, the deformation force yields to long-range chain slippage and the polymer instead exhibits flow behavior [40].

The gel contents of all PVA-based aerogels fabricated in this work were greater than 80%. The gel content of neat PVA and the PVA-MWCNT (1 wt%), PVA-MWCNT (2 wt%), and PVA-MWCNT (3 wt%) aerogels obtained

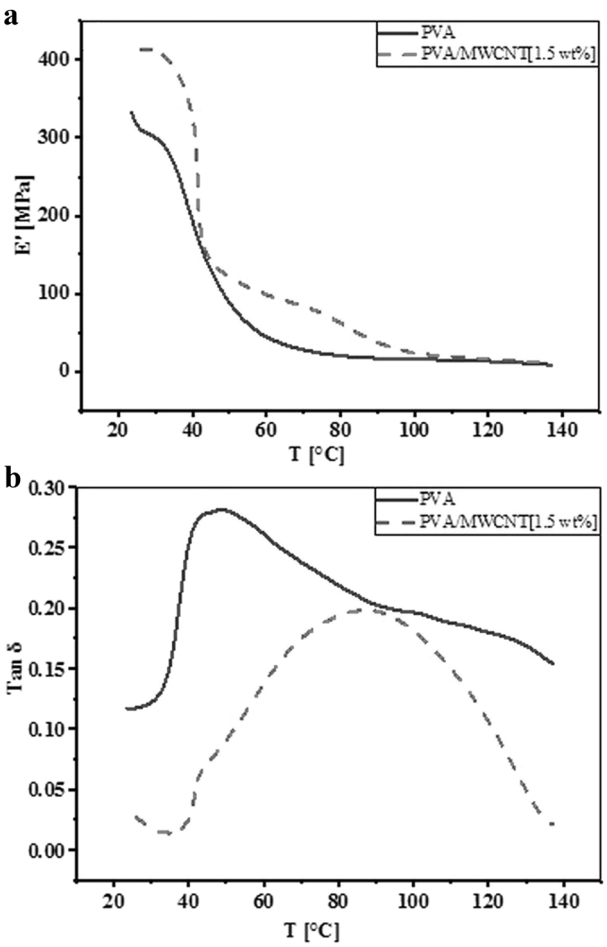

Fig. 4 **a** Storage modulus and **b** *tan δ* curves for PVA aerogel and the PVA-MWCNT (1.5 wt%) nanocomposite aerogel versus temperature

were 82%, 85%, 86%, and 87%, respectively. The gel contents of the nanocomposite aerogels increased by increasing the MWCNT loading levels. In addition to the presence of a polymer matrix, the introduction of MWCNTs significantly impacted the physical crosslinking in the aerogels. The crosslinks originated from the good interaction between the carbon nanotubes and PVA chains. The high gel contents (>80%) indicated that the crosslinking network required to observe the shape memory behavior had formed. Accordingly, heat treatment can strengthen PVA-based aerogels against water and improve their insolubility, thereby enhancing the applications of these materials, especially in aquatic media.

Using a Joule heating mechanism, the shape memory behavior of the aerogels in the thermally activated condition was quantitatively analyzed by observing the shape recovery process of the deformed samples at different recovery temperatures (90 and 95 °C) for 3 cycles. The glass transition temperature corresponded to the relaxation of the amorphous regions of the polymer, and thus, shape memory behavior was visible above the glass transition temperature T_g. In fact, the shape memory effect in polymers is an entropic phenomenon. In their permanent shape, polymer chains exhibit their highest level of entropy (the thermodynamically stable state). By heating the polymer chains to temperatures greater than T_g, the mobility of the polymer chains increased. When deformation forces were applied, the chains were deformation, forming a shape with a lower entropy state (temporary shape). Cooling below T_g froze the chains in this conformation, setting the temporary shape. In other words, by reducing the temperature beneath the transition temperature of the switching segments, the aerogel lacked sufficient energy to return autonomously to the disordered state of its original shape. When an SMP is heated above T_g, in the absence of any force, the chain mobility is reactivated, and the highest entropy state (permanent shape) can be recovered [40].

Figure 6 depicts the shape recovery procedure for the PVA/MWCNT (1 wt%) nanocomposite aerogel at 95 °C.

The shape memory results are summarized in Tables 3–5. The recovery time was found to gradually increase with increasing MWCNT content. This result was attributed to the strong interaction between the MWCNTs and amorphous chains of PVA, which resulted in the reduced chain mobility. By increasing the MWCNT content, the polymer chains no longer had sufficient time to unwrap and recover from the resultant nanocomposite aerogels. This led to longer recovery times of the nanocomposite aerogels compared to the neat PVA aerogel. A similar result was reported by Du et al. [2] for a PVA/MWCNT nanocomposite. Nevertheless, both the shape recovery ratio and recovery speed increased. The presence of MWCNTs was vital for improving the shape memory effect. As mentioned earlier, the nanotubes acted as a reinforcing agent, which gave rise to the increased storage modulus. In addition, by stabilizing the crystalline domains, the nanotubes can trigger a locking effect based on mechanical confinement [41]. As a direct result, the stiffness of the nanocomposite aerogel and its recovery stress increased. Accordingly, both the amount of energy absorbed and restoring energy were increased. By increasing the MWCNT content, the shape recovery ratio also improved (at 90 °C).

As a result of increasing the MWCNT content and, consequently, increasing the recovery time, it was expected that the recovery speed would decline; however, in contrast, the recovery speed was observed to increase. Apparently, the recovery speed was more sensible to changes in the recovery angle (the numerator of R_s) than recovery time (the denominator of R_s). By increasing the MWCNT content, the change in the recovery angle increased; therefore, the fraction of R_s would generally increase. In fact, it was not practical to achieve the desired recovery speed, because this parameter was determined according to the thermal

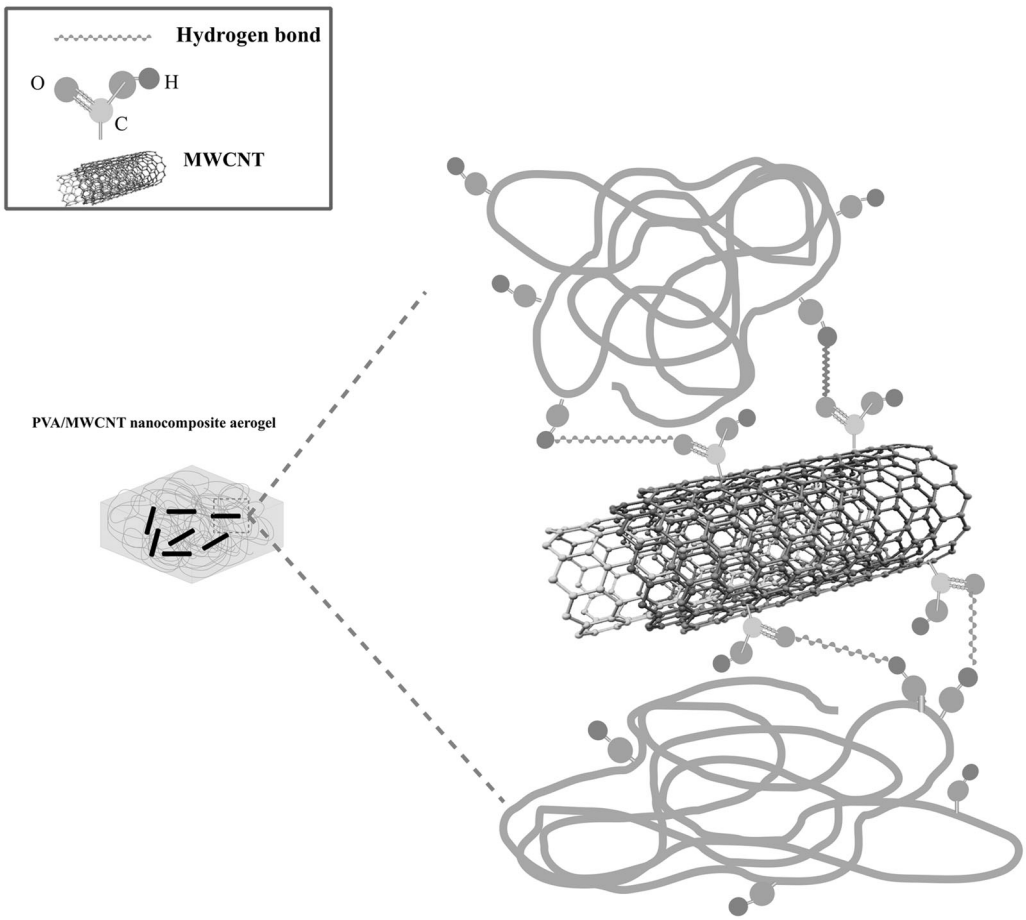

Fig. 5 Schematic illustration of the interaction between the PVA chains with the carboxylate groups of the MWCNTs

Fig. 6 Shape recovery of the PVA/MWCNT (1 wt%) nanocomposite aerogel at 95 °C

conductivity of the MWCNTs, heating procedure, ambient heat and other related factors.

Furthermore, increasing the recovery temperature (T_r) facilitated the shape recovery of all of the samples due to the increase in the mobility of the chains, Table 3. Higher values of T_r resulted in a higher shape recovery ratio (R_r) and shape recovery speed (R_s) but a shorter recovery time (t_r). By observing consecutive cycles, the nanocomposite aerogels were found to exhibit a perfect shape memory effect, even as the cycle number was increased, Tables 4 and 5. In other words, no significant decrease in either R_r or R_s was observed after the number of cycles tested here, and instead, both quantities remained almost constant. In fact, by repeating the thermomechanical shape memory cycle, not only was the PVA crosslinking network maintained, but upon the addition of a heating operation, the observed tendency was for the network to be reinforced. It is commonly known that an entropic elastic force is required as the driving force for SMP recovery to its original shape and this force can be achieved from the polymer network.

Conclusions

In this work, electrospun PVA/MWCNT aerogels were fabricated via the $ScCO_2$ drying method. The harvested PVA aerogel and PVA/MWCNT nanocomposite aerogels were fully characterized, and their shape memory behaviors were examined. SEM micrographs revealed the achievement of a nanofibrous network associated with

Table 3 Average values of R_r, R_s, and t_r for neat aerogel and nanocomposite aerogels in the first cycle

	$T_r = 90$ °C			$T_r = 95$ °C		
MWCNT content (wt%)	t_r (s)	R_r (%)	R_s (°/s)	t_r (s)	R_r (%)	R_s (%)
0	10 ± 0.01	85 ± 2	0.21 ± 4.8	8 ± 0.02	100	6.12 ± 0.03
1	17 ± 0.01	90 ±	0.06 ± 5.4	15 ± 0.01	100	7.37 ± 0.01
1.5	17 ± 0.02	92 ±	8.1 ± 0.18	16 ± 0.04	100	9.37 ± 0.02
2	20 ± 0.01	93 ±	7.7 ± 0.1	19 ± 0.03	100	10 ± 0.01
3	22 ± 0.03	96 ±	14 ± 0.1	22 ± 0.03	100	18.75 ± 0.01

Table 4 Average amount of R_r, R_s, and t_r for neat aerogel and nanocomposite aerogels in the second cycle

	$T_r = 90$ °C			$T_r = 95$ °C		
MWCNT content (wt%)	t_r (s)	R_r (%)	R_s (°/s)	t_r (s)	R_r (%)	R_s (°/s)
0	12 ± 0.02	85 ± 1	5 ± 0.1	12 ± 0.05	100	6.52 ± 0.03
1	17 ± 0.01	89 ± 1	5.68 ± 0.06	17 ± 0.01	100	7.5 ± 0.01
1.5	17 ± 0.01	92 ± 3	7.06 ± 0.18	17 ± 0.03	100	8.53 ± 0.01
2	22 ± 0.01	93 ± 2	7.65 ± 0.09	20 ± 0.04	100	8.23 ± 0.01
3	24 ± 0.02	96 ± 3	11.25 ± 0.13	23 ± 0.01	100	12.5 ± 0.01

Table 5 Average amount of R_r, R_s, and t_r neat aerogel and nanocomposite aerogels in the third cycle

	$T_r = 90$ °C			$T_r = 95$ °C		
MWCNT content (wt%)	t_r (s)	R_r (%)	R_s (°/s)	t_r (s)	R_r (%)	R_s (%)
0	13 ± 0.06	83 ± 2	4.58 ± 0.1	13 ± 0.04	100	5.6 ± 0.05
1	18 ± 0.07	86 ± 3	5.22 ± 0.05	17 ± 0.03	100	5.9 ± 0.1
1.5	24 ± 0.04	92 ± 3	5 ± 0.04	22 ± 0.03	100	6.36 ± 0.02
2	23 ± 0.03	93 ± 1	7.5 ± 0.12	22 ± 0.07	100	7.94 ± 0.01
3	24 ± 0.04	96 ± 4	9.62 ± 0.03	25 ± 0.01	100	10.77 ± 0.03

interconnected highly porous texture for all of the fabricated aerogels. The average size of the nanofibers in all of the samples was less than 100 nm. By embedding MWCNTs into the PVA matrix, the density and porosity of the aerogel increased and decreased slightly, respectively. These observations were attributed to the increased solid content of the aerogels. In addition, the specific surface area of the aerogels was reduced as the MWCNT loading level was increased. As the MWCNT content was increased to 1.5 wt%, the electrical conductivity increased abruptly by up to 4 orders of magnitude (3.62×10^{-7} S cm^{-1}), implying that an electrical percolation network had formed in the nanocomposite aerogels. AC electrical conductivity findings revealed an independent frequency region in the low-frequency range, which then increased at higher frequencies beyond the percolation threshold and was found to agree well with the DC results. By adding MWCNTs to PVA, the storage modulus and *tan δ* intensity increased and decreased, respectively, due to the reinforcing effect of the MWCNTs, which in turn impeded the chain mobility of the PVA. Furthermore, the shape memory results illustrated the shape recovery ratio, and the recovery speed of the nanocomposite aerogels increased, owing to the stabilizing of crystalline domains and improvements in the mechanical properties due to the addition of the MWCNTs.

Acknowledgements The authors wish to thank Tarbiat Modares University and the Iran Nanotechnology Initiative Council (INIC) for their support.

Compliance with ethical standards

Conflict of interest The authors declare that they have no conflict of interest.

References

1. Rezanejad S, Kokabi M. Shape memory and mechanical properties of cross-linked polyethylene/clay nanocomposites. Eur Polym J. 2007;43:2856–65.

2. Liu Y, Du H, Liu L, Leng J. Shape memory polymers and their composites in aerospace applications: a review. Smart Mater Struct. 2014;23:023001.
3. Vili YYFC. Investigating smart textiles based on shape memory materials. Text Res J. 2007;77:290–300.
4. Peterson GI, Dobrynin AV, Becker ML. Biodegradable shape memory polymers in medicine. Adv Heal Mater. 2017;6:1700694.
5. Kunzelman J, Chung T, Mather PT, Weder C. Shape memory polymers with built-in threshold temperature sensors. J Mater Chem. 2008;18:1082–6.
6. Meng Q, Hu J. A review of shape memory polymer composites and blends. Compos Part A. 2009;40:1661–72.
7. Li H, Zhong J, Meng J, Xian G. The reinforcement efficiency of carbon nanotubes/shape memory polymer nanocomposites. Compos Part B. 2013;44:508–16.
8. Zhao W, Gao C, Sang H, Xu J, Wang C, Wu Y. Calcium sulfate hemihydrate whisker reinforced polyvinyl alcohol with improved shape memory effect. RSC Adv. 2016;6:52982–6.
9. Du FP, Ye EZ, Tang CY, Ng SP, Zhou XP, Xie XL. Microstructure and shape memory effect of acidic carbon nanotubes reinforced polyvinyl alcohol nanocomposites. J Appl Polym Sci. 2013;129:1299–305.
10. Du H, Zhang J. Shape memory polymer based on chemically cross-linked poly(vinyl alcohol) containing a small number of water molecules. Colloid Polym Sci. 2010;288:15.
11. Miaudet P, Derré A, Maugey M, Zakri C, Piccione PM, Inoubli R, et al. Shape and temperature memory of nanocomposites with broadened glass transition. Science. 2007;318:1294–6.
12. Zhong J, Meng J, Yang Z, Poulin P, Koratkar N. Shape memory fiber supercapacitors. Nano Energy. 2015;17:330–8.
13. Basfar AA, Lotfy S. Radiation-crosslinking of shape memory polymers based on poly(vinyl alcohol) in the presence of carbon nanotubes. Radiat Phys Chem. 2015;106:376–84.
14. Du FP, Ye EZ, Yang W, Shen TH, Tang CY, Xie XL, et al. Electroactive shape memory polymer based on optimized multiwalled carbon nanotubes/polyvinyl alcohol nanocomposites. Compos Part B. 2015;68:170–5.
15. Wang L, Yang X, Chen H, Yang G, Gong T, Li W, et al. Multistimuli sensitive shape memory poly(vinyl alcohol)-graft-polyurethane. Polym Chem. 2013;4:4461–8.
16. Chen YN, Peng L, Liu T, Wang Y, Shi S, Wang H. Poly(vinyl alcohol)-tannic acid hydrogels with excellent mechanical properties and shape memory behaviors. ACS Appl Mater Interfaces. 2016;8:27199–206.
17. Nakagaito AN, Kondo H, Takagi H. Cellulose nanofiber aerogel production and applications. J Reinf Plast Compos. 2013;32:1547–52.
18. Li L, Yalcin B, Nguyen BN, Meador MAB, Cakmak M. Flexible nanofiber-reinforced aerogel (Xerogel) synthesis, manufacture, and characterization. ACS Appl Mater Interfaces. 2009;1:2491–501.
19. Farmer JC, Bahowick SM, Harrar JE, Fix DV, Martinelli RE, Vu AK, et al. Electrosorption of chromium ions on carbon aerogel electrodes as a means of remediating ground water. Energy Fuels. 1997;11:337–47.
20. Du A, Zhou B, Zhang Z, Shen J. A special material or a new state of matter: A review and reconsideration of the aerogel. Materials. 2013;6:941–68.
21. Takeshita S, Yoda S. Chitosan aerogels: transparent, flexible thermal insulators. Chem Mater. 2015;27:7569–72.
22. Paakko M, Vapaavuori J, Silvennoinen R, Kosonen H, Ankerfors M, Lindstrom T, et al. Long and entangled native cellulose I nanofibers allow flexible aerogels and hierarchically porous templates for functionalities. Soft Matter. 2008;4:2492–9.
23. Wu Z-Y, Li C, Liang H-W, Chen J-F, Yu SH. Ultralight, flexible, and fire-resistant carbon nanofiber aerogels from bacterial cellulose. Angew Chem Int Ed. 2013;125:2997–3001.
24. Hosseini H, Kokabi M, Mousavi SM. BC/rGO conductive nanocomposite aerogel as a strain sensor. Polymer. 2018;137:82–96.
25. Pereira AFG, Fernandes JV, Antunes JM, Sakharova NA. Shear modulus and Poisson's ratio of single-walled carbon nanotubes: numerical evaluation. Phys Status Solidi. 2016;253:366–76.
26. Shao LN, Dai J, Zhang ZX, Yang JH, Zhang N, Huang T, et al. Thermal and electroactive shape memory behaviors of poly (l-lactide)/thermoplastic polyurethane blend induced by carbon nanotubes. RSC Adv. 2015;5:101455–65.
27. Bang H, Gopiraman M, Kim BS, Kim SH, Kim IS. Effects of pH on electrospun PVA/acid-treated MWNT composite nanofibers. Colloids Surf A. 2012;409:112–7.
28. Jeong JS, Moon JS, Jeon SY, Park JH, Alegaonkar PS, Yoo JB. Mechanical properties of electrospun PVA/MWNTs composite nanofibers. Thin Solid Films. 2007;515:5136–41.
29. Dourani A, Hamadanian M, Haghgoo M, Jahannama MR, Goudarzi H. Morphology and electrical properties of multi-walled carbon nanotube/carbon aerogel prepared by using polyacrylonitrile as precursor. RSC Adv. 2015;5:49944–52.
30. Cai J, Kimura S, Wada M, Kuga S, Zhang L. Cellulose aerogels from aqueous alkali hydroxide–urea solution. ChemSusChem. 2008;1:149–54.
31. Zheng Q, Javadi A, Sabo R, Cai Z, Gong S. Polyvinyl alcohol (PVA)-cellulose nanofibril (CNF)-multiwalled carbon nanotube (MWCNT) hybrid organic aerogels with superior mechanical properties. RSC Adv. 2013;3:20816–23.
32. Worsley MA, Satcher JH, Baumann TF. Synthesis and characterization of monolithic carbon aerogel nanocomposites containing double-walled carbon nanotubes. Langmuir. 2008;24:9763–6.
33. Kohlmeyer RR, Lor M, Deng J, Liu H, Chen J. Preparation of stable carbon nanotube aerogels with high electrical conductivity and porosity. Carbon N Y. 2011;49:2352–61.
34. Sadeghi S, Arjmand M, Otero Navas I, Zehtab Yazdi A, Sundararaj U. Effect of nanofiller geometry on network formation in polymeric nanocomposites: comparison of rheological and electrical properties of multiwalled carbon nanotube and graphene nanoribbon. Macromolecules. 2017;50:3954–67.
35. Sun K, Xie P, Wang Z, Su T, Shao Q, Ryu J, et al. Flexible polydimethylsiloxane/multi-walled carbon nanotubes membranous metacomposites with negative permittivity. Polymer. 2017;125:50–7.
36. Wang M, Zhang K, Dai XX, Li Y, Guo J, Liu H, et al. Enhanced electrical conductivity and piezoresistive sensing in multi-wall carbon nanotubes/polydimethylsiloxane nanocomposites via the construction of a self-segregated structure. Nanoscale. 2017;9:11017–26.
37. Fritzsche J, Klüppel M. Structural dynamics and interfacial properties of filler-reinforced elastomers. J Phys. 2010;23:035104.
38. Wu TM, Chen EC, Lin YW, Chiang MF, Chang GY. Preparation and characterization of melt-processed polycarbonate/multiwalled carbon nanotube composites. Polym Eng Sci. 2008;48:1369–75.
39. Park OK, Lee JH. Carbon nanotube-poly (vinyl alcohol) hybrid aerogels: Improvements in the surface area and structural stability by internal morphology control. Compos Part B. 2018;144:229–36.
40. Xie T. Recent advances in polymer shape memory. Polymer. 2011;52:4985–5000.
41. Viry L, Mercader C, Miaudet P, Zakri C, Derre A, Kuhn A, et al. Nanotube fibers for electromechanical and shape memory actuators. J Mater Chem. 2010;20:3487–95.